Atmospheric
Chemistry
and Physics
Discussions

Open Access

An empirically derived inorganic sea spray source function incorporating sea surface temperature

M. E. Salter[1], P. Zieger[1], J. C. Acosta Navarro[1], H. Grythe[1,2,3], A. Kirkevåg[4], B. Rosati[5], I. Riipinen[1], and E. D. Nilsson[1]

[1]Stockholm University, Department of Environmental Science and Analytical Chemistry, 11418 Stockholm, Sweden
[2]Norwegian Institute for Air Research, P.O. Box 100, 2027 Kjeller, Norway
[3]Finnish Meteorological Institute, Air Quality Research, Erik Palmenin aukio 1, P.O. Box 503, 00101 Helsinki, Finland
[4]Norwegian Meteorological Institute, P.O. Box 43, Blindern, 0313 Oslo, Norway
[5]Paul Scherrer Institute, Laboratory of Atmospheric Chemistry, 5232 Villigen, Switzerland

Discussion Paper | Discussion Paper | Discussion Paper | Discussion Paper

ACPD

15, 13783–13826, 2015

A sea spray source function incorporating SST

M. E. Salter et al.

Title Page

Abstract | Introduction

Conclusions | References

Tables | Figures

|◄ | ►|

◄ | ►

Back | Close

Full Screen / Esc

Printer-friendly Version

Interactive Discussion

Abstract

We have developed an inorganic sea spray source function that is based upon state-of-the-art measurements of sea spray aerosol production using a temperature-controlled plunging jet sea spray aerosol chamber. The size-resolved particle production was measured between 0.01 and 10 µm dry diameter. Particle production decreased non-linearly with increasing seawater temperature (between −1 and 30 °C) similar to previous findings. In addition, we observed that the particle effective radius as well as the particle-surface, -volume and -mass, increased with increasing seawater temperature due to increased production of super-micron particles. By combining these measurements with the volume of air entrained by the plunging jet we have determined the size-resolved particle flux as a function of air entrainment. Through the use of existing parameterisations of air entrainment as a function of wind speed we were subsequently able to scale our laboratory measurements of particle production to wind speed. By scaling in this way we avoid the difficulties associated with defining the "white-area" of the laboratory whitecap – a contentious issue when relating laboratory measurements of particle production to oceanic whitecaps using the more frequently applied whitecap method.

The here-derived inorganic sea spray sea spray source function was implemented in a Lagrangian particle dispersion model (FLEXPART). An estimated annual global flux of inorganic sea spray aerosol of $5.9 \pm 0.2\,\mathrm{Pg\,yr^{-1}}$ was derived that is close to the median of estimates from the same model using a wide range of existing sea spray source functions. When using the source function derived here, the model also showed good skill in predicting measurements of Na^+ concentration at a number of field sites further underlining the validity of our source function.

In a final step, the sensitivity of a large-scale model (NorESM) to our new source function was tested. Compared to the previously implemented parameterisation, a clear decrease of sea spray aerosol number flux and increase in aerosol residence time was observed, especially over the Southern Ocean. At the same time an increase in aerosol

optical depth due to an increase in the number of particles with optically relevant sizes was found. That there were noticeable regional differences may have important implications for aerosol optical properties and number concentrations, subsequently also affecting the indirect radiative forcing by non-sea spray anthropogenic aerosols.

1   Introduction

Primary marine aerosol or sea spray aerosol particles (SSA) are those particles produced directly at the ocean surface following wave breaking, air entrainment as bubbles, and the subsequent bubble bursting process at the ocean surface (Lewis and Schwartz, 2004). When considered in terms of mass, sea spray aerosol particles constitute the largest flux of particulate matter to the atmosphere after wind-blown dust, with a global production of 3 to 30 Pg yr^{-1} (Lewis and Schwartz, 2004).

Sea spray aerosol is important for the climate system where it acts as both a direct and indirect radiative forcing component (Stocker et al., 2013). Both of these forcing effects are highly dependent upon the total number and size distribution parameters of the emitted sea spray aerosol particles; the direct effect is dominated by airborne particulate surface area while the indirect effect is more closely related to the number of particles above a given size. Thus, sea spray aerosol properties have been the subject of significant scientific debate, centred on both the environmental factors that might affect the production of sea spray aerosol and the best experimental approach to estimate the source function of sea spray aerosol particles emitted (Lewis and Schwartz, 2004; de Leeuw et al., 2011).

Although wind speed is the major driver of air entrainment into surface waters, simply parameterising sea spray aerosol production in terms of wind speed often fails to reconcile predicted and observed sea spray aerosol concentrations (e.g. Grythe et al., 2014). Secondary factors such as wave state and sea surface temperature (SST) are known to affect a host of processes from initial air entrainment to the final production of sea spray aerosol droplets and these may in part explain these discrepancies. They

may also explain some of the disparity between different sea spray aerosol source parameterisations (de Leeuw et al., 2011).

A number of recent findings have highlighted the potential importance of sea surface temperature on sea spray aerosol production. Salter et al. (2014) have shown that the interfacial bubble flux and bubble size spectra are strongly dependent on water temperature and that these are strongly correlated to total particle number flux in a laboratory setting. Grythe et al. (2014) noted a strong influence of sea surface temperature on sea spray aerosol production when they compared existing sea spray aerosol source functions with a global database of sea spray aerosol mass concentration measurements. Salisbury et al. (2014) noted large differences between a commonly used whitecap fraction parameterisation (Monahan and O'Muircheartaigh, 1980) derived almost entirely in low-latitude regions and a satellite estimate derived over the entire globe. The authors postulate that the weaker wind speed dependence observed in their global dataset may in part be due to the influence of secondary factors which co-vary with the wind geographically, such as sea surface temperature. Their data indicated that at a given wind speed, the satellite-derived whitecap fraction decreases with increasing sea surface temperature (see Fig. 9 in Salisbury et al., 2013).

Much of the discussion on the role of sea surface temperature in sea spray aerosol production has focused on the apparent contradiction between observations made using laboratory systems that attempt to replicate oceanic whitecaps and observations of sea salt concentrations made in the field or inferred from aerosol optical depth (AOD) measurements. A series of laboratory systems designed to replicate sea spray aerosol production by whitecaps have shown that the number production flux increases markedly as water temperatures are decreased (e.g. Salter et al., 2014; Zábori et al., 2013; Bowyer et al., 1990). In contrast, observational data from the field, such as chemical analysis of particulate matter smaller than 10 μm (PM_{10}) or total suspended mass, have often been used to infer that sea spray aerosol production increases with higher sea surface temperatures due to higher observed concentrations at lower latitudes (e.g. Jaeglé et al., 2011; Grythe et al., 2014). Similarly, Sofiev et al. (2011) noted a bias

A sea spray source function incorporating SST

M. E. Salter et al.

between predictions of sea spray aerosol induced aerosol optical depth and measurements of aerosol optical depth when using a sea spray source function not dependent on sea surface temperature. They noted that the aerosol optical depth determined near the tropics using a sea spray aerosol source function without sea surface temperature dependence was a factor of 2 lower than observations of aerosol optical depth, suggesting that sea spray aerosol production was underestimated at lower latitudes where sea surface temperatures are higher and wind speed is generally lower.

One explanation for the aforementioned contradiction could be the distinct properties of the sea spray aerosol that the different approaches measure. In the laboratory studies, emphasis has been placed on obtaining estimates of the number production flux of particles. The majority of these studies have focused on particles smaller than 1 µm dry diameter, both through system design and instrumental restrictions, but also because this size range dominates sea spray aerosol number production. However, particles with dry diameter larger than 1 µm provide the dominant contribution to the fluxes of surface area and volume; thus, these particles are the most important for applications involving light scattering and particle mass. Consequently, studies that infer a temperature dependence of sea spray aerosol production fluxes based upon sea salt concentrations (determined from PM_{10} data) and aerosol optical depth measurements in the field are likely to be highly influenced by the latter properties. The incongruity between laboratory studies and aerosol optical depth/sea salt mass studies may simply result from changes to the size distribution of sea spray aerosol coincident with changes to the total number production flux as seawater temperature changes.

To test this hypothesis we have determined the particle number flux in the size range 0.01 to 10 µm dry diameter (D_p) in a temperature-controlled laboratory sea spray chamber. This setup previously highlighted a significant dependence of particle number concentration ($D_p \geq 0.01$ µm) on water temperature, with significant increases at lower water temperatures (Salter et al., 2014). However, during these experiments this system was not optimised to measure larger particles and suffered from significant particles losses for particles $D_p \gtrsim 3$ µm. Therefore, in order to obtain better comparisons with

measurements of PM_{10}, we have improved both the sampling protocol and the instrumentation used to measure particles with D_p larger than 1 µm (Sect. 3). Using this new data we have derived a sea spray aerosol source function (Sect. 4) and compared it to field measurements using a Lagrangian particle dispersion model (FLEXPART; Stohl et al., 2005, see Sect. 5). Finally, we have deployed the new parameterisation in an Earth system model (NorESM; Kirkevåg et al., 2013, see Sect. 6) to facilitate comparison with the previous temperature dependent parameterisation.

2   Methods

2.1   The sea spray chamber

In order to observe the effects of sea surface temperature on the source flux of aerosol produced, we have utilised a temperature controlled sea spray generation chamber. This system has been described in detail by Salter et al. (2014). However, a number of modifications were made to the system to improve estimates of the aerosol particle production flux, especially for particles with $D_p > 1$ µm.

The sea spray chamber is fabricated from stainless steel components and incorporates temperature control (±0.1 °C) so that the water temperature can be held constant between −1 and 30 °C. Air was entrained using a plunging jet that exited a stainless steel nozzle with inner diameter 4.3 mm held in a vertical position 30 cm above the air–water interface. Water was circulated from the centre of the bottom of the tank back through this nozzle using a peristaltic pump (Watson–Marlow, 620S) and silicone tubing. All surfaces below the water level on the inside of the tank were coated in Teflon, and prior to all experiments all internal surfaces were rinsed thoroughly with reagent grade ethanol and low-organic-carbon (American Society for Testing and Materials Type 1) standard deionised water (> 18.2 MΩ), hereafter referred to as DIW.

Both seawater salinity and temperature were measured continuously using an Aanderaa 4120 conductivity sensor. Seawater dissolved oxygen concentration was mea-

sured with an Aanderaa oxygen optode 4175. This sensor also provided an independent temperature measurement. Both sensors were placed towards the centre of the tank approximately halfway between the tank base and the air–water interface. Relative humidity and temperature were measured in the headspace of the sea spray simulator using a Vaisala model HMT333 probe.

Dry zero sweep air entered the tank at $6\,\mathrm{L\,min^{-1}}$ after passing through an ultrafilter (Type H cartridge, MSA) and an activated carbon filter (Ultrafilter, AG-AK). The airflow rate was maintained and quantified using a mass flow controller (Brooks, 5851S). Aerosol particle-laden air was sampled through a number of ports in the lid of the sea spray simulator and transferred under laminar flow to all aerosol instrumentation. To prevent contamination by room air, the sea spray simulator was operated under slight positive pressure by maintaining the sweep-air flow several $\mathrm{L\,min^{-1}}$ greater than the sampling rate. Excess air was vented through a 1-way flutter valve on the lid of the system.

2.2 Particle size distribution measurements

2.2.1 Differential mobility particle sizer and condensation particle counter

Aerosol particle-laden air was directed through $2\,\mathrm{m}$ of $1/4''$ stainless steel tubing and a custom made silica diffusion dryer at which point the flow was split. Immediately following this split a TSI model 3010 condensation particle counter (CPC) was used to enumerate the total number concentration at $1\,\mathrm{Hz}$ for particles with $D_\mathrm{p} > 0.01\,\mathrm{\mu m}$. The aerosol particle-laden air which entered the second sampling line was first directed to a custom made impactor ($0.0707\,\mathrm{cm}$ nozzle, with a cutoff diameter of $\sim 1\,\mathrm{\mu m}$ at $1\,\mathrm{L\,min^{-1}}$), it was then passed through a bipolar charger (neutralizer, Ni-63.), before it entered a closed-loop sheath air, custom-built differential mobility particle sizer (DMPS) which selected negatively charged particles using a positive high voltage in the differential mobility analyser (DMA). The selected particles were enumerated with a TSI 3772 CPC ($1\,\mathrm{L\,min^{-1}}$ flow rate). The DMPS was used to determine the size distribution for

the size range $0.01\,\mu m < D_p < 0.7\,\mu m$ (electrical mobility diameter) and a single scan over 37 size bins was completed in 12 minutes.

A particle's mobility equivalent diameter, D_{mob}, is defined as the diameter of a sphere with the same electrical mobility as the particle. D_{mob} is only equal to the volume equivalent diameter, D_{ve}, for spherical particles. Since NaCl and the other salts present in the artificial seawater used during our study form cubic and not spherical particles when aerosolised and dried, we have shape corrected the mobility diameters obtained using our DMPS. The relation between D_{mob} and D_{ve} of a particle is:

$$f = \frac{D_{ve}}{D_{mob}} = \frac{1}{\chi} \frac{C_c(D_{ve})}{C_c(D_{mob})} \qquad (1)$$

where f is the correction factor applied to each diameter measured, χ is the dynamic shape factor of the particle, and C_c is the Cunningham slip correction factor (Hinds, 1999). For spherical particles, χ has by definition the value 1, while for NaCl χ is equal to 1.08 or that of a cube (Hinds, 1999). We assume that this value holds for the artificial sea salt used during our experiments and have used it to correct the size distributions obtained with our DMPS system to volume equivalent diameters.

2.2.2 White-light optical particle size spectrometer

Aerosol particle-laden air was vertically sampled and drawn directly upwards, without bends or contractions in the sample line, through 0.75 m of $1/2''$ stainless steel tubing and a custom made silica diffusion dryer to a Palas WELAS 2300 white-light aerosol spectrometer (WELAS; Palas GmbH) that was mounted directly above the sea spray chamber. This is an optical particle size spectrometer (OPSS) with a white-light source (Osram XBO-75 Xenon short arc lamp in the wavelength range of $\lambda \approx 350\text{–}750\,nm$) that illuminates a measuring volume of $\sim 7\,cm^{-3}$. Optical lenses collect the scattered light between 78 and 102° with respect to the incident beam and direct it to a photomultiplier tube (PMT). The sensor is connected to the light source and detector via optical fibers which minimises heat input from the lamp and temperature increase in

A sea spray source function incorporating SST

M. E. Salter et al.

Title Page

Abstract	Introduction
Conclusions	References
Tables	Figures

|◀ ▶|

◀ ▶

Back Close

Full Screen / Esc

Printer-friendly Version

Interactive Discussion

the sensor. This instrument was used to obtain the aerosol size distribution for the size range $0.2\,\mu m < D_p < 10\,\mu m$ (polystyrene latex sphere optical equivalent diameter) at 1 Hz, sizing particles in 59 bins.

Given that the OPSS instrument employs a white-light source it should be less in-fluenced by so called "Mie wiggles" than OPSS instruments which use monochromatic light sources. Thus, the OPSS should be less affected by sizing ambiguities than a sin-gle wavelength OPSS.

The OPSS reports equivalent optical diameters which were calculated by the in-strument's firmware using a preset empirical calibration curve based on polystyrene latex (PSL) sphere measurements. In order to account for systematic instrumental drifts caused by changes in the incident light intensity, changes of the PMT efficiency, or degradations of the optical fibers, we made periodic measurements of $0.85\,\mu m$ monodisperse Caldust (Calibration Dust provided by the manufacturer). Using these measurements the instruments firmware applied a correction factor to maintain a con-stant relation between scattered light intensity and optical diameter.

The probability that the OPSS will detect a particle is a function of the particle's size or cross section resulting in a size dependant counting efficiency. For particles close to the small end of the OPSS sizing range there is a decreased probability of detection or counting efficiency. Rosati et al. (2015) have determined the counting efficiency of the OPSS used in this study and their results were similar to those of Mullins et al. (2012). One hundred percent counting efficiency is attained for all particles larger than $0.3\,\mu m$, and the counting efficiency increases to a maximum of $\sim 130\%$. The raw counts ob-tained by the OPSS were multiplied by the reciprocal of the counting efficiency curve generated by Rosati et al. (2015) to correct for the counting efficiency of the instrument.

As with all OPSS instruments, the OPSS measurements depend on the wavelength-dependent complex refractive index of the sampled aerosol. It is this that determines the scattering response for particles of a given size and shape. Therefore, measure-ment of non-PSL aerosols such as sea salt aerosol particles with an OPSS factory calibrated with PSLs will manifest in a diameter shift of the size distribution due to dif-

ferences in the refractive index of the materials. Since this diameter shift is likely to have a large influence on the aerosol particle surface and volume size distributions, we have corrected for it assuming that the sea salt aerosol particles had a refractive index of $m = 1.54 - 0i$ (Abo Riziq et al., 2007) which corresponds to the value of NaCl (compared to a refractive index of $m = 1.588 - 0i$ for the PSLs the instrument was calibrated with).

As with the DMPS measurements, there is also an effect of particle shape on the OPSS measurements. Therefore, these measurements were also corrected, through the use of PALAS PDAnalyze software, assuming that the shape factor of 1.08 for NaCl holds for the artificial sea salt used during these experiments.

2.2.3 Temperature and humidity of the sampled aerosol

The temperature and relative humidity (RH) of the sample entering the DMPS, as well as the sheath air of the DMPS were monitored using a Campbell Scientific HMP50 sensor. Although the relative humidity of the air entering the OPSS instrument was not measured directly, it is assumed that it was always well below 30 % such that the sea spray aerosol had effloresced. This conclusion was made on the basis that all driers were of identical design and because the flow through the OPSS drier was significantly lower than the flow through the DMPS drier (OPSS: $0.5\,\mathrm{L\,min^{-1}}$; DMPS: $2\,\mathrm{L\,min^{-1}}$). Based upon the dimensions of the diffusion driers used and the flow rates of the various instruments, the residence time of the aerosol particle-laden air in the driers was ∼ 6 s, and ∼ 1.5 s for the OPSS, and DMPS instruments respectively. The silica gel in each drier was replaced when the relative humidity measured at the inlet to the DMPS exceeded 25 %. Therefore, we report our aerosol in dry diameters.

2.3 Experimental setup

Each experiment was conducted with artificial seawater (ASW) consisting of Sigma sea salt (Sigma Aldrich, S9883; mass fraction: 55 % Cl^-, 31 % Na^+, 8 % SO_4^{2-}, 4 % Mg^{2+},

1 % K^+, 1 % Ca^{2+}, < 1 % other) rehydrated to an absolute salinity of 35 g Kg^{-1} using DIW. We subjected our artificial seawater to a purification process in the same manner as previously described by Salter et al. (2014). This consisted of activated charcoal treatments, artificial UV exposures and hydrogen peroxide (H_2O_2, 30 % solution, no stabilizer) additions. Here H_2O_2 acted as an oxidising agent to remove organic matter.

Manipulating the water temperature in the sea spray chamber could potentially have changed gas saturation levels in the water. Since there has been speculation in the literature that sub- or super-saturations of atmospheric gases in seawater might affect particle production through changes to the bubble population (e.g. Stramska et al., 1990), we conducted constant temperature experiments to ensure that gas saturations were in thermodynamic equilibrium with the headspace of the sea spray chamber. Once the artificial seawater purification procedure was complete, the water temperature was held constant at a series of values between −1 and 30 °C whilst measurements of the aerosol generated were conducted. The water temperatures investigated were −1, 3, 5, 8, 10, 20, and 30 °C. At each water temperature aerosol measurements were conducted over a period ≥ 2 h following a period of at least 12 h at the desired temperature. Measurements of oxygen concentration in the seawater confirmed that gas saturations were in thermodynamic equilibrium and the oxygen % saturations were not significantly different between the experiments. The mean oxygen saturation across all experiments was 111 % with a standard deviation of 1 % (the reported accuracy of the Aanderaa oxygen optode 4175 is to within < 5 % saturation), within the range of anomalies typically encountered in ocean surface waters (Najjar and Keeling, 1997).

The second phase of the experiment consisted of measurements of the sea spray aerosol particles generated whilst the temperature of the water was slowly ramped downward from 30 to 2 °C over a period of 29 h. This second phase was conducted 24 h after the first phase of experiments were completed. In the interim period the chamber was kept closed with a constant in-flow of zero-particle air and the same water was used for both experiments. At no point during the seawater cooling experiment was the water undersaturated with respect to O_2 (see Supplement), nor was it signifi-

cantly different than the mean of the constant temperature experiments (mean oxygen saturation: 111 %).

2.4 Model simulations

2.4.1 The FLEXPART Lagrangian particle dispersion model

The FLEXPART Lagrangian particle dispersion model (Stohl et al., 2005) has been used to simulate sea spray aerosol transport from its source to a series of observations sites where chemical analysis of Na^+ on aerosol filter samples has been conducted. This model computes the trajectories of particles in the atmosphere to describe the transport and turbulent diffusion of tracers. In this study particles were released from the observation sites at a constant rate of 15000 particles per hour during every measurement sampling interval and followed backwards in time for 20 days. When run in backward mode tracing mass concentrations the output of the model is an emission sensitivity in seconds as a function of space (1° × 1° with variable vertical resolution) and time (every 3 h). By multiplying the emission sensitivity in the lowest model layer (100 m) by a source flux the source contribution is obtained which when integrated over all grid cells and 3 hour intervals provides the simulated sea spray aerosol concentration at the measurement point averaged over the sampling interval. Further detail on the manner in which we run this model can be found in Grythe et al. (2014).

In order to facilitate comparison with other commonly deployed sea spray source functions, four lognormal modes with modal diameters of 1.3, 9.4, 13.6, and 17.8 µm and corresponding geometric standard deviations of 1.350, 1.100, 1.075, and 1.050 were used to approximate the source function presented in Sect. 4.

FLEXPART modelled sea spray aerosol concentrations using the parameterisation presented in this study are compared with the database of observed sea spray aerosol concentrations compiled by Grythe et al. (2014). This consists of observational data obtained at 21 monitoring sites and on-board ships during 11 research cruises (see

Table 1 in Grythe et al., 2014) and totals over 20000 observations distributed over the global oceans.

2.5 The NorESM Earth system model

We have used a modified first version of the Norwegian Earth System Model, NorESM1-M (Bentsen et al., 2013; Iversen et al., 2013; Kirkevåg et al., 2013). This model is run with intermediate atmospheric resolution ($1.9° \times 2.5°$) and is based on the CCSM4 model developed at NCAR (Gent et al., 2011). The model was set up to run in the same manner as described by Kirkevåg et al. (2013) with only slight modifications to the version of the atmospheric model, CAM4-Oslo. The model was set up using pre-scribed sea surface temperatures and run in offline mode, so that changes in aerosol treatment do not affect the meteorology.

The aerosol module in the atmospheric model, CAM4-Oslo, describes the size-resolved aerosol physics and transport of 20 aerosol components and combines a life-cycle model which handles the emissions, processing and transport of aerosol mass combined with a physics scheme with look-up tables calculated by an offline micro-physics model. The look-up tables are used to compute the bulk (from size-resolved) physical and optical properties of the aerosol population. The differences introduced in the aerosol schemes compared to Kirkevåg et al. (2013) are the modified modal median diameters and standard deviations of the lognormal (and dry) sea spray size distributions at the point of emission. The new size parameters are listed in Table 1. The previous modal median diameters for the three modes were 0.044, 0.26, and 1.48 µm and the previous standard deviations were 1.59, 1.59, 2.0.

3 Results

3.1 Measured number size distributions during the constant temperature experiments

Over the 0.01 to 10 µm diameter size range covered by the DMPS system and OPSS instrument, when represented in the form $dN/d\log D_p$, the size distributions obtained during the constant water temperature experiments exhibit three modes (Fig. 1). A noteworthy observation is the apparent lack of agreement between the DMPS measurements and the OPSS measurements in the particle size range where they overlap. This is despite correcting both instruments for particle shape and correcting the OPSS instrument for the likely influence of particle refractive index. Both of these corrections only influence the sizing of the particles and have no influence on the number of particles counted by the instruments. Most likely the DMPS instrument was increasingly influenced by particle losses due to the system tubing and the impactor placed before it in its upper sizing range. It should be borne in mind that the particle size range over which the instruments disagree is not dominating $dN/d\log D_p$, $dS/d\log D_p$ or $dV/d\log D_p$ so it is unlikely to influence the number fluxes, optical properties, or mass fluxes of the sea spray source function derived later in this study.

Following correction for the effect of shape, the DMPS system data exhibited a single mode centred close to 0.1 µm when plotted in the form $dN/d\log D_p$. This mode decreased in number as the water temperature was increased between –1 and 30 °C. Following correction for the effect of both shape and refractive index, the data obtained using the OPSS exhibited two modes when plotted in the form $dN/d\log D_p$. One was centred around 0.55 µm and another was centred around 1.5 µm. The mode centred around 0.55 µm exhibited similar behaviour to the mode centred around 0.1 µm in that it decreased in number as the water temperature increased. However, the mode centred around 1.5 µm exhibited different behaviour in that it increased in number as the water temperature was increased. This effect is much more prominent when the size distribution is plotted in the form of the particle surface size distribution $dS/d\log D_p$ or

particle volume size distribution $dV/d\log D_p$ which both assume that the particles are spherical (Fig. 1).

Also noteworthy is the observation that the data obtained at 30 °C appears to show a sudden shift in the size distribution to larger sizes. Although we cannot discount that this effect is real, that we observe this effect only at a water temperature of 30 °C suggests that this is more likely to have been a measurement artifact. Given that at a water temperature of 30 °C in the chamber the air temperature was only slightly lower and the sea spray chamber headspace had an RH of ∼ 98 %, the absolute water content will have been high. This combined with the observed increase in the number of larger particles (> 1 µm) at this temperature relative to lower water temperatures may mean that despite the fact that the RH at the inlet to the OPSS was below the efflorescence point of the particles, assuming they were mainly NaCl, the particles may not have had adequate time to fully effloresce and thus could have still been partially liquid. The rate at which the particles were crystallising may also have changed, a factor which is known to effect the ultimate shape NaCl particles take when dried (Wang et al., 2010).

3.2 Measured number size distributions during the temperature ramp experiments

Once the constant temperature experiments were complete, an experiment where the temperature of the water was slowly ramped downward from 30 to 2 °C over a period of 29 h was conducted. In order to obtain estimates of the particle size distributions as a function of water temperature during this experiment the data were binned at a resolution of 1 °C. Here the data from the DMPS system and the OPSS have been combined following corrections for particle shape and refractive index respectively. The two instruments both provide size resolved particle number in the dry diameter range between ∼ 0.2 to 0.7 µm. Given that for particles close to the small end of the OPSS sizing range there is a decreased probability of detection and that an increasing number of particles close to upper size range of the DMPS system will have been influenced by

the ~ 1 µm impactor placed prior to it, we have chosen to use the DMPS measurements in the range 0.01 to 0.45 µm and the OPSS measurements in the range 0.45 to 10 µm.

Measured $dN/d\log D_p$ was very similar to the constant temperature experiments, consisting of three modes centred at dry diameters of ~ 0.1, ~ 0.55, and ~ 1.5 µm (see Supplement). The two smallest modes decreased in magnitude with increased water temperature whilst the mode at the largest dry diameter exhibited opposite behaviour and increased in number as the water temperature was increased. Once again this trend is much more apparent when the size distribution is presented in the forms $dS/d\log D_p$ and $dV/d\log D_p$. The sudden shift towards larger particles observed in the constant temperature experiments was also apparent during the temperature ramp experiments. However, it appeared at a slightly lower temperature of ~ 23 °C.

Comparison of the constant temperature experiments and the temperature ramp experiments is facilitated in Fig. 2. The integrated total particle number concentration (integrated across the size range 0.01 to 10 µm) in the temperature ramp experiments was not significantly different to the constant temperature experiments. Figure 2d plots the effective radius (r_{eff}) of both the constant temperature experiments and the temperature ramp experiment as a function of water temperature where:

$$r_{eff} = \frac{3V}{A} \tag{2}$$

where V is the total integrated particle volume and A is the total integrated particle surface area (assuming spherical particles). The effective radius of both the constant temperature experiments and the temperature ramp experiment were also very similar at comparable water temperatures.

Given the observed similarity between the constant water temperature experiments and the water temperature ramp experiments as well as the higher water temperature resolution of the latter experiments, we have chosen to use the data from only the temperature ramp experiments to generate a new inorganic sea spray aerosol parameterisation as a function of water temperature in the following section.

4 Derivation of a model parameterisation of the sea spray aerosol production flux

4.1 Air entrainment as a function of wind speed

We have combined the number of particles in a unit logarithmic interval of D_p produced per unit time ($p(D_p, T)$) as a function of seawater temperature measured during our experiments with measurements of the air entrained by the plunging jet as a function of temperature presented in Salter et al. (2014). This approach is based on the assumption that all air entrained into the water column detrains as bubbles that produce particles. Thus, the size-resolved particle production flux measured in the sea spray chamber as a function of water temperature during our experiments ($f_\tau(D_p, T)$) is defined as:

$$f_\tau(D_p, T) = \frac{p(D_p, T)}{\tau(T)} \tag{3}$$

where $p(D_p, T)$ is the number of particles in a unit logarithmic interval of D_p produced per unit time as a function of water temperature (T) and $\tau(T)$ is the rate of air entrainment in $m^3 s^{-1}$ as a function of water temperature.

In order to estimate the size-resolved oceanic interfacial sea spray aerosol production flux, we have combined the size-resolved particle production flux from Eq. (3) with an estimate of the entrainment flux of air into the oceanic water column in the same manner as described by Long et al. (2011):

$$f_{int}(D_p, T) = f_\tau(D_p, T) F_{ent} \tag{4}$$

where F_{ent} is the dependence of the air entrainment flux into the oceanic water column on wind speed measured at 10 m height (U_{10}).

As discussed by Long et al. (2011), the air entrainment flux into the water column (F_{ent}) can be estimated from

$$F_{ent} = \alpha \epsilon_d \tag{5}$$

where e_d is the rate of energy dissipation by wave breaking in $\mathrm{W\,m^{-2}}$ and α is the ratio of the volume of air entrained by breaking waves to the energy dissipated by the wind-wave through wave breaking. As presented by Long et al. (2011), initially we assumed a range of $(4 \pm 2) \times 10^{-4}\,\mathrm{m^3\,J^{-1}}$ for α and that e_d varies as a function of wind speed as $(5 \pm 1) \times 10^{-5}(U_{10})^{3.74}\,\mathrm{W\,m^{-2}}$ giving

$$F_{ent} = (2 \pm 1) \times 10^{-8} \cdot (U_{10})^{3.74} \tag{6}$$

where F_{ent} is in $\mathrm{m^3\,m^{-2}\,s^{-1}}$. However, this resulted in unrealistic over-production of sea spray aerosol at low latitudes in the Southern Hemisphere when implemented in the Earth system model, NorESM (see Sect. 6). Numerous existing sea spray aerosol parameterisations based upon the whitecap method utilise a wind speed dependence of $(U_{10})^{3.41}$ with recent studies advocating even lower wind speed dependencies with a smaller exponent for U_{10} (e.g. Callaghan, 2013). Given this we have kept the scaling to air entrainment the same as that used by Long et al. (2011) but use a lower wind speed dependency of $(U_{10})^{3.41}$, which is the same value used by Kirkevåg et al. (2013). This results in a final dependency of air entrainment on wind speed of

$$F_{ent} = 2(\pm 1) \times 10^{-8} \cdot (U_{10})^{3.41} \tag{7}$$

where F_{ent} is in $\mathrm{m^3\,m^{-2}\,s^{-1}}$.

4.2 Effective vs. interfacial sea spray aerosol fluxes

The aim of this study is to provide a parameterisation of sea spray aerosol production to represent the production flux in atmospheric chemical transport models or global circulation models. Usually such models have their lowest atmospheric layer at 10 m and often much higher (e.g. 100 and 180 m in FLEXPART and NorESM, respectively). Therefore, knowledge of the size distribution of particles that attain significant height in the atmosphere, often referred to as the effective flux, is required. Since the inlets

A sea spray source function incorporating SST

M. E. Salter et al.

Title Page

Abstract | Introduction

Conclusions | References

Tables | Figures

◄ | ►

◄ | ►

Back | Close

Full Screen / Esc

Printer-friendly Version

Interactive Discussion

to the aerosol instrumentation used during this study were sited ~ 30 cm above the water surface we have determined the flux of particles that reached this height, often referred to as the interfacial flux. As such, consideration should be given to the difference between the effective production flux and the interfacial production flux measured at ~ 30 cm.

Using an approach described by Lewis and Schwartz (2004) we have attempted to convert the interfacial fluxes measured in the sea spray chamber utilised during this study to effective fluxes at 10 m height. This approach is outlined in detail in the Supplement accompanying this work. Since the ratio of effective fluxes to interfacial fluxes depends on both particle size and wind speed, computation of the effective sea spray aerosol particle flux should take into account both variables. However, since it would be computationally expensive to compute the ratio of effective fluxes to interfacial fluxes on the fly in Earth system models, we have converted the temperature dependent interfacial fluxes measured during our study to temperature dependent effective fluxes based upon a single wind speed (U_{10}) of 7 m s^{-1}, approximately the global average wind speed over the ocean. Although an implication of this assumption is that effective fluxes may be overestimated at wind speeds below 7 m s^{-1} and underestimated at wind speeds above 7 m s^{-1}, we expect this effect to be negligible compared to the alternative of simply implementing interfacial fluxes into models.

4.3 Size distribution as a function of temperature

Using the data presented in Sect. 3.2 we have generated a temperature dependent sea spray source function. Since the majority of Earth system models utilise modal modules as input for aerosol emissions to limit computation time, we present our source function in this manner. A large number of these models are limited to three lognormal modes that are fixed to prescribed size-ranges with fixed model diameters and geometric standard deviations. Therefore, we present a source function consistent with this approach.

The effective particle production flux (see Fig. 3) has been parameterized by fitting the 1 °C binned interfacial number fluxes obtained during the temperature ramp experiments corrected to an effective flux at $7\,\mathrm{m\,s^{-1}}$ wind speed, to the sum of three lognormal distributions of the form:

$$\frac{\mathrm{d}F}{\mathrm{d}\log D_{\mathrm{p}}} = \sum_{i=1}^{3} \frac{N_i}{\sqrt{2\pi}\log\sigma_i} \exp\left(-\frac{1}{2}\frac{(\log D_{\mathrm{p}} - \log\bar{D}_{\mathrm{mod},i})^2}{\log\sigma_i}\right) \tag{8}$$

where N_i is the number production flux, $\bar{D}_{\mathrm{mod},i}$ is the mode (median) diameter, σ_i is the standard deviation of the ith lognormal mode, and log is the logarithm with base 10.

Least-squares polynomial curve fitting was conducted to allow estimation of the number production flux (N_i) of the lognormal modes, with fixed modal diameters and geometric standard deviations, as a function of water temperature. Therefore, in the final form of the parameterisation, the number production flux (N_i) of each of the three lognormal modes is a cubic function of sea surface temperature:

$$N_i = F_{\mathrm{ent}(U_{10})} \cdot (A_i \cdot T^3 + B_i \cdot T^2 + C_i \cdot T + D_i) \tag{9}$$

where $F_{\mathrm{ent}(U_{10})}$ is the volume of air entrained as a function of U_{10} (Eq. 7) and T is the sea surface temperature in Celsius. Table 1 describes the details of the three modes and the modal emission coefficients for use in Eq. (9).

Figure 3 depicts the number effective fluxes, per cubic metre of air entrained, determined from the temperature ramp data (see Sect. 3.2) using the approach described earlier in this section. Overlaid in black are the lognormal fits for each water temperature obtained when the modal diameters and geometric standard deviations were fixed to the values given in Table 1 and the number fluxes were estimated using the polynomial coefficients given in Table 1 using Eq. (9). Generally the fits are able to account for most of the variability in the measured number effective flux distributions, with the coefficient of determination (R^2) values of the fits ranging between 0.94 and 0.97 for the effective number fluxes across the range of temperatures 2 to 30 °C. Comparison

between the predicted surface area fluxes and those measured highlight discrepancies, however. Between 2 and 22 °C the correlation between predicted surface area fluxes and those measured is generally good with R^2 values between 0.96 and 0.99. However, at water temperatures higher than 22 °C the correlation between predicted surface area fluxes and those measured becomes much poorer, with R^2 values decreasing monotonically from 0.70 at 23 °C to 0.21 at 30 °C. This disconnect results from the fact that the measured particles increase considerably in size, an effect which the fits, constrained to constant modal diameter and geometric standard deviations, cannot account for. The observation that a transition to larger particle sizes occurred at a water temperature of $\sim$ 23 °C was discussed in detail in Sect. 3.1 with the conclusion that we cannot exclude that the particles had not fully effloresced at these higher water temperatures. Given this, we have assumed that the small increase in the number of super-micron particles observed as water temperatures increased from 2 to 22 °C continued at higher water temperatures by simply extrapolating the increase in the number production flux in the fitted mode centred at 1.5 µm observed in the water temperature between 2 and 22 up to 30 °C.

The source function estimated during this study is compared with a variety of source functions from other recent studies for wind speeds of 10 m s^{-1} in panel a of Fig. 4 (Mårtensson et al., 2003; Gong, 2003; Long et al., 2011; Clarke et al., 2006) as well as the previous source function implemented in the Earth system model, NorESM described by Kirkevåg et al. (2013). The latter source function is a slight modification of the previous sea spray aerosol treatment in NorESM1-M introduced by Struthers et al. (2013), which in turn was based on the Mårtensson et al. (2003) source function. Therefore, it includes a dependence on sea surface temperatures. In contrast, the source functions of Gong (2003), Long et al. (2011) and Clarke et al. (2006) do not incorporate a dependence on sea surface temperature and were presumably derived at water temperatures somewhere close to either room temperature (in the case of Long et al., 2011; Gong, 2003) or to the sea surface temperature in coastal Hawaii (in the case of Clarke et al., 2006) since none of the studies make specific reference to the

A sea spray source function incorporating SST

M. E. Salter et al.

Title Page

Abstract   Introduction

Conclusions   References

Tables   Figures

|◄   ►|

◄   ►

Back   Close

Full Screen / Esc

Printer-friendly Version

Interactive Discussion

water temperature. All the source functions are shown for particle sizes normalised to dry diameter. The source function obtained during this study lies within the range of the other functions for all particle sizes measured.

Assuming the measured sea spray aerosol particles are spherical it is possible to integrate the sea spray aerosol mass flux to obtain mass emissions as a function of wind speed and sea surface temperature. This can then be compared to observations as well as previously published sea spray aerosol source functions. Sea spray aerosol mass emissions, $\bar{F}$ can be obtained as follows:

$$\bar{F} = \frac{\pi}{6}\rho_{ss}\int_{D_{p,1}}^{D_{p,2}}\frac{dF}{d\log D_p}D_p{}^3 dD_p \tag{10}$$

where ρ_{ss} is the density of sea salt, $2.16\,\mathrm{g\,cm^{-3}}$ assuming it is similar to that of NaCl. Panel b in Fig. 4 shows sub-micron $\bar{F}$ (integrated across the size range: $0.029\,\mu m < D_p < 0.580\,\mu m$) as a function of wind speed for the sea spray source function derived during this study at sea surface temperatures of 2, 15, and 30 °C, a number of previously published source functions, the source function previously implemented in the Earth system model, NorESM described by Kirkevåg et al. (2013), as well as a fit to measurements made at the Mace Head coastal station recently published by Ceburnis et al. (2014). It is clear from these figures that the previously published source functions, including the source function previously implemented in NorESM, overpredict sub-micron sea salt mass emissions to the extent that at $U_{10} = 10\,\mathrm{m\,s^{-1}}$ they are all at least a factor of ~ 3 too high. The Long et al. (2011) source function overpredicts by an order of magnitude at $U_{10} = 10\,\mathrm{m\,s^{-1}}$ in part due to its strong wind speed dependence of $(U_{10})^{3.74}$. This appears to support our decision to reduce the wind speed dependence of our function down from $(U_{10})^{3.74}$ to $(U_{10})^{3.41}$. Indeed, the new source function presented in this study compares much better with the measurements of Ceburnis et al. (2014).

5 Comparison to a Lagrangian particle dispersion model

Using European Centre for Medium-Range Weather Forecasts (ECMWF) wind fields over a 25 yr period, sea spray aerosol production was calculated using the source function presented here as well as a number of source functions more commonly deployed in large scale models. Annual mean global sea spray aerosol production was 5.9 ± 0.2 Pg yr^{-1}. Although this is at the low end of the range of estimates presented by Grythe et al. (2014) of between 1.83 and 2444 Pg yr^{-1} it compares favourably with the median of the 22 source functions of 5.91 Pg yr^{-1} (Grythe et al., 2014). For comparison the source functions of Monahan et al. (1986), Gong (2003), and Sofiev et al. (2011) produced 4.5, 4.6, and 2.6 Pg yr^{-1}, respectively. Further comparison to existing source functions can be made using Table 2 in Grythe et al. (2014).

FLEXPART modelled sea spray aerosol concentrations using the parameterisation presented in this study can be compared with the database of observed sea spray aerosol concentrations compiled by Grythe et al. (2014). This consists of observational data obtained at 21 monitoring sites and on-board ships during 11 research cruises (see Table 1 in Grythe et al., 2014) and totals over 20000 observations distributed over the global oceans. Figure 5 compares FLEXPART modelled with measured Na$^+$ concentrations using the sea spray source function presented here for four stations included in the comparison, Barrow, Malin Head, Valentia, and Zeppelin. The Pearson's correlation coefficient when comparing measured and modelled concentrations at these four stations is 0.79 which compares favourably with those of other common parameterisations when the same comparison was conducted by Grythe et al. (2014) of between 0.42 and 0.81. However, the performance of the model using the source function presented here ranged considerably across the four stations – lower skill was observed at the two polar stations, Barrow, Alaska, and Zeppelin, Svalbard, which are characterised by lower concentrations of Na$^+$ overall. Their distance from large open seawater sources relative to Malin Head and Valentia as well as the higher elevation of Zeppelin (475 m above sea level) may mean that they are less representa-

tive of fresh sea spray aerosol. The Pearson's correlation coefficient when comparing the entire data set is 0.4, whilst it is 0.3, 0.8, and 0.3 when comparing only PM_{10} measurements, EMEP station observations, and weekly observations, respectively. The value for the entire dataset compares favourably with the correlations between modelled and observed sea spray aerosol concentrations for other common sea spray aerosol parameterisations found by Grythe et al. (2014). Here correlations ranged between 0.16 and 0.41 when comparing the entire data set.

It is clear from Fig. 5 that the model is biased $\sim 50\%$ low compared to the measurements. A low bias of similar magnitude was observed for many commonly deployed source functions tested by Grythe et al. (2014). It may be caused by the proximity of the observations to coastal wave breaking in the form of surf which is not accounted for in the models, as well as inadequate treatment of sea spray aerosol post production in the model. For example, errors in the rate of below cloud aerosol scavenging in the model will have knock-on effects on the aerosol residence time and how much of the aerosol produced by wave breaking was predicted to reach the point of measurement.

6 Global simulations using an Earth system model

We ran a total of three two-year NorESM simulations after one year of spinup. The model was set-up as atmosphere-only and the atmosphere was coupled with the data ocean and sea-ice model (from CCSM4). In addition, the CAM4-Oslo aerosol life cycle module was run offline with respect to the atmospheric component so that the aerosol changes induced by changing sea spray aerosol emissions in CAM4-Oslo had no effect on the meteorology in any of the simulations. We chose not to include these feedbacks in order to obtain a clearer causal relation between sea surface temperature and sea spray aerosol given that all of these runs had exactly the same meteorology. All simulations employ emissions of SO_2, SO_4, particulate organic matter, and black carbon from fossil-fuel and bio-fuel combustion and biomass burning, taken from the IPCC

AR5 data sets as in Kirkevåg et al. (2013). The description of the runs and the sea spray parametrisation is presented in Table 2.

The global sea spray aerosol mass emission predicted by the model using the sea spray source function presented in this study is $1.84 \pm 0.92 \, \mathrm{Pg \, yr^{-1}}$ whilst the global sea spray aerosol number emission is $210\,000 \pm 105\,000 \, \mathrm{particles \, m^{-2} \, s^{-1}}$ based on the uncertainty in oceanic air entrainment presented by Long et al. (2011). Although the global sea spray aerosol mass emission predicted by NorESM is significantly lower than that predicted by the Lagrangian particle dispersion model, FLEXPART, the reader should be aware that comparison between different model estimates is not direct. This is because the different models have different assumptions for the sea spray size representation. NorESM uses the three modes described in Table 1, whilst FLEXPART used four lognormal distributions with modal diameters of 1.3, 9.4, 13.6, and 17.8 µm and corresponding geometric standard deviations of 1.350, 1.100, 1.075, 1.050, respectively to approximate the source function (as well as all others in the comparison).

To determine the influence of including a dependence on sea surface temperature in the sea spray aerosol source function relative to no dependence on sea surface temperature we ran a simulation where the sea surface temperature was fixed at 15 °C over the entire ocean. Figure 6 plots the difference in sea spray aerosol number flux, mass flux and clear-sky aerosol optical depth at 550 nm between the run with variable sea surface temperatures and the run with sea surface temperatures fixed at 15 °C (the variable sea surface temperature run minus the fixed sea surface temperature run). Sea spray aerosol number fluxes are slightly larger at higher latitudes in the Northern Hemisphere and significantly larger at higher latitudes in the Southern Hemisphere when a temperature dependence is included. There is no discernible difference at lower latitudes in both hemispheres. When a temperature dependence is included, sea spray aerosol mass fluxes are slightly higher throughout the entire Northern Hemisphere whilst they are significantly lower at higher latitudes in the Southern Hemisphere. Clear-sky aerosol optical depth values (panel c in Fig. 6) are also generally higher in the Northern Hemisphere, when a sea surface temperature dependence is included, es-

pecially around the tropics which is consistent with the observations of Sofiev et al. (2011). Averaged globally over a year, including a dependence on sea surface temperature in the sea spray source function decreases sea spray aerosol mass fluxes by $\sim 7\%$, increases sea spray aerosol number fluxes by $\sim 14\%$, and increases clear-sky aerosol optical depth by $< 0.1\%$ relative to a fixed sea surface temperature of $15\,°C$. These results highlight the potential importance of including a dependence on sea surface temperature in the sea spray source function.

Panel a in Fig. 7 compares sea spray aerosol number concentrations modelled by NorESM using both the previous sea spray source function and that presented in the current study. From this figure it is clear the changing the sea spray parameterisation decreases the sea spray aerosol number concentration in the model in the lowest atmospheric layer. Over the Southern Ocean the effect is particularly noticeable – there are significantly less sea spray aerosol particles in the lowest layers of the model atmosphere in the model run using the parameterisation developed during this study when compared to the Kirkevåg et al. (2013) parameterisation.

Further evaluation of the new parameterisations deployment within NorESM is facilitated through comparison of modelled clear-sky aerosol optical depth at 550 nm in panel b of Fig. 7. Across all regions in the Northern Hemisphere there is no discernible difference between all three model runs due to the dominance of aerosols other than sea spray aerosol. However, there are significant differences at higher latitudes in the Southern Hemisphere. Here, the model run using the sea spray aerosol parameterisation developed during this study and climatology sea surface temperatures simulates increased clear-sky aerosol optical depth.

It is also useful to consider the total column burden of sea spray aerosol (C_{SSA}), the sea spray aerosol residence time, as well as the sea spray aerosol mass specific extinction (ME) which is defined as the sea spray aerosol optical depth divided by the sea spray aerosol column burden. A comparison of these parameters between the previous parameterisation and that proposed in the current study is facilitated in Fig. 8 and Table 3. The column burdens of sea salt aerosol are generally lower in the parameter-

A sea spray source function incorporating SST

M. E. Salter et al.

isation proposed in this study compared to the previous parameterisation of Kirkevåg et al. (2013) apart from in the polar regions. Globally averaged sea spray aerosol column burdens are 7.44 and 7.42 mg m^{-2} for the parameterisation with climatology sea surface temperatures and sea surface temperature fixed at 15 °C, respectively, compared to 9.74 mg m^{-2} with the previous parameterisation deployed in NorESM (Table 3). The parameterisation developed during this study results in slightly increased numbers of accumulation mode particles across all latitudes but decreased amounts of super-micron particles which dominate the mass production – hence the decreased total column burden. The current parameterisation results in significantly larger sea spray aerosol mass specific extinction and longer residence times than the previous parameterisation which is to be expected given that the effective radii of the sea spray aerosol are closer to the accumulation mode in the current parameterisation. The global mean residence time of 69.9 h (median of 29.6 h) for the current parameterisation and 23.5 h (median of 10 h) for the previous parameterisation can be compared with the AeroCom model comparison study (Textor et al., 2006) where the mean residence time for sea spray aerosol was modelled as 12 h (median of 7.2 h) with an inter-model diversity of 59 %. The sea spray aerosol residence time resulting from the new parameterisation is therefore outside the AeroCom model diversity interval. Our calculated sea spray aerosol column burdens do however fall within the range of values reported by Textor et al. (2006) which has a mean of 15.5 mg m^{-2} (median of 12.7 mg m^{-2}) and an inter-model diversity of 69 %. Kinne et al. (2006) also report sea spray aerosol optical depth and mass specific extinction for the AeroCom models. These values vary between 0.003 and 0.067 (median 0.030) for optical depth, and between 0.88 and 7.5 m^2 g^{-1} (median 3 m^2 g^{-1}) for mass specific extinction. Compared with Kinne et al. (2006), our calculated sea salt aerosol optical depth of 0.038 and mass specific extinction of 5.1 m^2 g^{-1} also fall within the inter-model diversities of AeroCom. In essence, the changes to the modal diameters coincident with changes to the magnitudes of the fluxes of each mode compensate, resulting in decreased sea spray aerosol number, increased residence time, and increased clear-sky aerosol optical depth compared to

the previous parameterisation deployed in the model. When viewed as a whole these changes to the sea spray aerosol parameterisation are likely to have important implications for aerosol optical properties and number concentrations, subsequently also affecting the indirect radiative forcing by (non-sea spray) anthropogenic aerosols (e.g. Hoose et al., 2009), especially at the regional level.

7 Conclusions

We have developed a parameterisation for inorganic sea spray aerosol production based upon state-of-the-art measurements of aerosol production using a temperature-controlled laboratory sea spray aerosol chamber. Using measurements of particle production in the size range 0.01 to 10 μm dry diameter we observed that particle production decreased non-linearly with increasing seawater temperature (between −1 and 30 °C) similar to previous findings. In addition, we observed that the particle effective radius as well as the particle-surface, -volume and -mass, increased with increasing water temperature due to increased production of super-micron particles. These observations might explain the contradiction between observations made using laboratory systems that attempt to replicate oceanic whitecaps, where decreasing particle production with increasing seawater temperature is observed, and observations of sea salt concentrations made in the field or inferred from aerosol optical depth measurements which tend to increase with increasing seawater temperature.

We have combined our measurements of particle production with measurements of the volume of air entrained by the plunging jet in order to determine the size-resolved particle flux as a function of air entrainment. By scaling in this way we avoid the difficulties associated with defining the "white-area" of the laboratory whitecap – a contentious issue when using the more frequently applied whitecap method.

The here-derived inorganic sea spray sea spray source function was implemented in a Lagrangian particle dispersion model. An estimated annual global flux of inorganic sea spray aerosol of $5.9 \pm 0.2\,\mathrm{Pg\,yr^{-1}}$ was derived that is close to the median

of estimates from the same model using a wide range of existing sea spray source functions. When using the source function derived here, the model also showed good skill in predicting measurements of Na$^+$ concentration at a number of field sites further underlining the validity of our source function.

In a final step, the sensitivity of a large-scale model to our new source function was tested by implementing it in the Earth system model, NorESM. Compared to the previously implemented parameterisation, a clear decrease of sea spray aerosol number flux and increase in aerosol residence time was observed, especially over the Southern Ocean. At the same time an increase in aerosol optical depth due to an increase in the number of particles with optically relevant sizes was found. That there were noticeable regional differences may have important implications for aerosol optical properties and number concentrations, subsequently also affecting the indirect radiative forcing by non-sea spray anthropogenic aerosols.

The Supplement related to this article is available online at doi:10.5194/acpd-15-13783-2015-supplement.

References

Abo Riziq, A., Erlick, C., Dinar, E., and Rudich, Y.: Optical properties of absorbing and non-absorbing aerosols retrieved by cavity ring down (CRD) spectroscopy, Atmos. Chem. Phys., 7, 1523–1536, doi:10.5194/acp-7-1523-2007, 2007. 13792

Bentsen, M., Bethke, I., Debernard, J. B., Iversen, T., Kirkevåg, A., Seland, Ø., Drange, H., Roelandt, C., Seierstad, I. A., Hoose, C., and Kristjánsson, J. E.: The Norwegian Earth System Model, NorESM1-M – Part 1: Description and basic evaluation of the physical climate, Geosci. Model Dev., 6, 687–720, doi:10.5194/gmd-6-687-2013, 2013. 13795

Bowyer, P. A., Woolf, D. K., and Monahan, E. C.: Temperature dependence of the charge and aerosol production associated with a breaking wave in a whitecap simulation tank, J. Geophys. Res., 95, 5313–5319, doi:10.1029/JC095iC04p05313, 1990. 13786

Callaghan, A.: An improved whitecap timescale for sea spray aerosol production flux modeling using the discrete whitecap method, J. Geophys. Res., 118, 9997–10010. doi:10.1002/jgrd.50768, 2013. 13800

Ceburnis, D., Rinaldi, M., Keane-Brennan, J., Ovadnevaite, J., Martucci, G., Giulianelli, L., , and O'Dowd, C. D.: Marine submicron aerosol sources, sinks and chemical fluxes, Atmos. Chem. Phys. Discuss., 14, 23847–23889, doi:10.5194/acpd-14-23847-2014, 2014. 13804, 13822

Clarke, A. D., Owens, S. R., and Zhou, J. C.: An ultrafine sea-salt flux from breaking waves: Implications for cloud condensation nuclei in the remote marine atmosphere, J. Geophys. Res., 111, D06202, doi:10.1029/2005JD006565, 2006. 13803, 13822

de Leeuw, G., Andreas, E. L., Anguelova, M. D., Fairall, C. W., Lewis, E. R., O'Dowd, C. D., Schulz, M., and Schwartz, S. E.: Production flux of sea spray aerosol, Rev. Geophys., 49, RG2001, doi:10.1029/2010RG000349, 2011. 13785, 13786

Gent, P. R., Danabasoglu, G., Donner, L. J., Holland, M. M., Hunke, E. C., Jayne, S. R., Lawrence, D. M., Neale, R. B., Rasch, P. J., Vertenstein, M., Worley, P. H., Yang, Z., and Zhang, M.: The community climate system model version 4, J. Climate, 24, 4973–4991, doi:10.1175/2011JCLI4083.1, 2011. 13795

Gong, S. L.: A parameterization of sea-salt aerosol source function for sub- and super-micron particles, Global Biogeochem. Cy., 17, 1097, doi:10.1029/2003GB002079, 2003. 13803, 13805, 13822

Grythe, H., Ström, J., Krejci, R., Quinn, P., and Stohl, A.: A review of sea-spray aerosol source functions using a large global set of sea salt aerosol concentration measurements, Atmos.

A sea spray source function incorporating SST

M. E. Salter et al.

Title Page

Abstract	Introduction
Conclusions	References
Tables	Figures

Back | Close

Full Screen / Esc

Printer-friendly Version

Interactive Discussion

Chem. Phys., 14, 1277–1297, doi:10.5194/acp-14-1277-2014, 2014. 13785, 13786, 13794, 13795, 13805, 13806, 13823

Hinds, W.: Aerosol Technology: Properties, Behavior, and Measurement of Airborne Particles, John Wiley & Sons, New York, 1999. 13790

5 Hoose, C., Kristjansson, J. E., Iversen, T., Kirkevåg, A., Seland, Ø., and Gettelman, A.: Constraining cloud droplet number concentration in GCMs suppresses the aerosol indirect effect, Geophys. Res. Lett., 36, L12807, doi:10.1029/2009GL038568, 2009. 13810

Iversen, T., Bentsen, M., Bethke, I., Debernard, J. B., Kirkevåg, A., Seland, Ø., Drange, H., Kristjansson, J. E., Medhaug, I., Sand, M., and Seierstad, I. A.: The Norwegian Earth System

10 Model, NorESM1-M – Part 2: Climate response and scenario projections, Geosci. Model Dev., 6, 389–415, doi:10.5194/gmd-6-389-2013, 2013. 13795

Jaeglé, L., Quinn, P. K., Bates, T. S., Alexander, B., and Lin, J.-T.: Global distribution of sea salt aerosols: new constraints from in situ and remote sensing observations, Atmos. Chem. Phys., 11, 3137–3157, doi:10.5194/acp-11-3137-2011, 2011. 13786

15 Kinne, S., Schulz, M., Textor, C., Guibert, S., Balkanski, Y., Bauer, S. E., Berntsen, T., Berglen, T. F., Boucher, O., Chin, M., Collins, W., Dentener, F., Diehl, T., Easter, R., Feichter, J., Fillmore, D., Ghan, S., Ginoux, P., Gong, S., Grini, A., Hendricks, J., Herzog, M., Horowitz, L., Isaksen, I., Iversen, T., Kirkevåg, A., Kloster, S., Koch, D., Kristjansson, J. E., Krol, M., Lauer, A., Lamarque, J. F., Lesins, G., Liu, X., Lohmann, U., Montanaro, V.,

20 Myhre, G., Penner, J., Pitari, G., Reddy, S., Seland, O., Stier, P., Takemura, T., and Tie, X.: An AeroCom initial assessment – optical properties in aerosol component modules of global models, Atmos. Chem. Phys., 6, 1815–1834, doi:10.5194/acp-6-1815-2006, 2006. 13809

Kirkevåg, A., Iversen, T., Seland, Ø., Hoose, C., Kristjánsson, J. E., Struthers, H., Ekman, A. M. L., Ghan, S., Griesfeller, J., Nilsson, E. D., and Schulz, M.: Aerosol–climate

25 interactions in the Norwegian Earth System Model – NorESM1-M, Geosci. Model Dev., 6, 207–244, doi:10.5194/gmd-6-207-2013, 2013. 13788, 13795, 13800, 13803, 13804, 13807, 13808, 13809, 13817, 13822, 13826

Lewis, E. R. and Schwartz, S. E.: Sea Salt Aerosol Production: Mechanisms, Methods, Measurements and Models – a Critical Review, Geophys. Monogr., Vol. 152, Amer. Geophys.

30 Union, 2004. 13785, 13801

Long, M. S., Keene, W. C., Kieber, D. J., Erickson, D. J., and Maring, H.: A sea-state based source function for size- and composition-resolved marine aerosol production, Atmos. Chem.

Title Page

Abstract | Introduction

Conclusions | References

Tables | Figures

|◀ | ▶|

◀ | ▶

Back | Close

Full Screen / Esc

Printer-friendly Version

Interactive Discussion

Phys., 11, 1203–1216, doi:10.5194/acp-11-1203-2011, 2011. 13799, 13800, 13803, 13804, 13807, 13822

Mårtensson, E. M., Nilsson, E. D., de Leeuw, G., Cohen, L. H., and Hansson, H. C.: Laboratory simulations and parameterization of the primary marine aerosol production, J. Geophys. Res., 108, 4297, doi:10.1029/2002JD002263, 2003. 13803, 13822

Monahan, E. C. and O'Muircheartaigh, I.: Optimal power-law description of oceanic whitecap coverage dependence on wind speed, J. Phys. Oceanogr., 10, 2094–2099, doi:10.1175/1520-0485(1980)010<2094:OPLDOO>2.0.CO;2, 1980. 13786

Monahan, E. C., Spiel, D. E., and Davidson, K. L.: Oceanic Whitecaps, in: A Model of Marine Aerosol Generation Via Whitecaps and Wave Disruption, 167–174, D. Reidel Publishing Company, 1986. 13805

Mullins, B. J., Kampa, D., and Kasper, G.: Comment on "Performance evaluation of 3 optical particle counters with an efficient multimodal calibration method" (Heim et al., 2008) – Performance of improved counter, J. Aerosol Sci., 49, 48–50, doi:10.1016/j.jaerosci.2012.01.009, 2012. 13791

Najjar, R. G. and Keeling, R. F.: Analysis of the mean annual cycle of the dissolved oxygen anomaly in the World Ocean, J. Marine Res., 55, 117–151, doi:10.1357/0022240973224481, 1997. 13793

Rosati, B., Wehrle, G., Gysel, M., Zieger, P., Baltensperger, U., and Weingartner, E.: The white-light humidified optical particle spectrometer (WHOPS) – a novel airborne system to characterize aerosol hygroscopicity, Atmos. Meas. Tech., 8, 921–939, doi:10.5194/amt-8-921-2015, 2015. 13791

Salisbury, D. J., Anguelova, M. D., and Brooks, I. M.: On the variability of white-cap fraction using satellite-based observations, J. Geophys. Res., 118, 6201–6222, doi:10.1002/2013JC008797, 2013. 13786

Salisbury, D. J., Anguelova, M. D., and Brooks, I. M.: Global distribution and seasonal dependence of satellite-based whitecap fraction, Geophys. Res. Lett., 41, 1616–1623, doi:10.1002/2014GL059246, 2014. 13786

Salter, M. E., Nilsson, E. D., Butcher, A., and Merete, B.: On the seawater temperature dependence of continuous plunging jet derived sea spray aerosol, J. Geophys. Res., 119, 9052–9072, doi:10.1002/2013JD021376, 2014. 13786, 13787, 13788, 13793, 13799

Title Page

Abstract | Introduction

Conclusions | References

Tables | Figures

|◄ | ►|

◄ | ►

Back | Close

Full Screen / Esc

Printer-friendly Version

Interactive Discussion

Sofiev, M., Soares, J., Prank, M., de Leeuw, G., and Kukkonen, J.: A regional-to-global model of emission and transport of sea salt particles in the atmosphere, J. Geophys. Res., 116, D21302, doi:10.1029/2010JD014713, 2011. 13786, 13805, 13808

Stocker, T. F., Qin, D., Plattner, G. K., Tignor, M., Allen, S. K., Boschung, J., Nauels, A., Xia, Y., Bex, V., and Midgley, P. M.: Climate Change 2013: The Physical Science Basis. Contribution of Working Group I to the Fifth Assessment Report of the Intergovernmental Panel on Climate Change, Cambridge Univ. Press, Cambridge, UK and New York, USA, 2013. 13785

Stohl, A., Forster, C., Frank, A., Seibert, P., and Wotawa, G.: Technical note: The Lagrangian particle dispersion model FLEXPART version 6.2, Atmos. Chem. Phys., 5, 2461–2474, doi:10.5194/acp-5-2461-2005, 2005. 13788, 13794

Stramska, M., Marks, R., and Monahan, E. C.: Bubble-mediated aerosol production as a consequence of wave breaking in supersaturated (hyperoxic) seawater, J. Geophys. Res., 95, 18281–18288, doi:10.1029/JC095iC10p18281, 1990. 13793

Struthers, H., Ekman, A. M. L., Glantz, P., Iversen, T., Kirkevåg, A., Seland, Ø., Martensson, E. M., Noone, K., and Nilsson, E. D.: Climate-induced changes in sea salt aerosol number emissions: 1870 to 2100, J. Geophys. Res., 118, 670–682, doi:10.1002/jgrd.50129, 2013. 13803

Textor, C., Schulz, M., Guibert, S., Kinne, S., Balkanski, Y., Bauer, S., Berntsen, T., Berglen, T., Boucher, O., Chin, M., Dentener, F., Diehl, T., Easter, R., Feichter, H., Fillmore, D., Ghan, S., Ginoux, P., Gong, S., Grini, A., Hendricks, J., Horowitz, L., Huang, P., Isaksen, I., Iversen, I., Kloster, S., Koch, D., Kirkevåg, A., Kristjansson, J. E., Krol, M., Lauer, A., Lamarque, J. F., Liu, X., Montanaro, V., Myhre, G., Penner, J., Pitari, G., Reddy, S., Seland, Ø., Stier, P., Takemura, T., and Tie, X.: Analysis and quantification of the diversities of aerosol life cycles within AeroCom, Atmos. Chem. Phys., 6, 1777–1813, doi:10.5194/acp-6-1777-2006, 2006. 13809

Wang, Z., King, S. M., Freney, E., Rosenoern, T., Smith, M. L., Chen, Q., Kuwata, M., Lewis, E. R., Pöschl, U., Wang, W., Buseck, P. R., and Martin, S. T.: The dynamic shape factor of sodium chloride nanoparticles as regulated by drying rate, Aerosol Sci. Tech., 44, 939–953, doi:10.1080/02786826.2010.503204, 2010. 13797

Zábori, J., Krejci, R., Ström, J., Vaattovaara, P., Ekman, A. M. L., Salter, M. E., Mårtensson, E. M., and Nilsson, E. D.: Comparison between summertime and wintertime Arctic Ocean primary marine aerosol properties, Atmos. Chem. Phys., 13, 4783–4799, doi:10.5194/acp-13-4783-2013, 2013. 13786

A sea spray source function incorporating SST

M. E. Salter et al.

Title Page

Abstract	Introduction
Conclusions	References
Tables	Figures

| ◄ | ► |
| ◄ | ► |

Back | Close

Full Screen / Esc

Printer-friendly Version

Interactive Discussion

Table 1. Modal diameters, geometric standard deviations (σ), and the polynomial coefficients for the number flux (N_i) of each of the three lognormal modes (Eq. 9).

Mode	Modal diameter (µm)	σ	A_i	B_i	C_i	D_i
1	0.095	2.10	-5.2168×10^5	3.31725×10^7	-6.95275×10^8	1.0684×10^{10}
2	0.6	1.72	0.00	7.374×10^5	-2.4803×10^7	7.7373×10^8
3	1.5	1.60	0.00	1.4210×10^4	1.4662×10^7	1.7075×10^8

Table 2. Description of the simulated sensitivity experiments conducted in NorESM. The simulated climate was identical in all experiments.

Run	Sea surface temperature	Wind speed at 10 m	SSA wind speed dependency[a]	Sea spray parametrisation
1	Varying (from climatology)	Varying (computed online)	$F_{ent} = 2 \times 10^{-8} U_{10}^{3.41}$	This study
2	Fixed at 15 °C in all gridcells	Varying (computed online)	$F_{ent} = 2 \times 10^{-8} U_{10}^{3.41}$	This study
3	Varying (from climatology)	Varying (computed online)	$W = 3.84 \times 10^{-6} U_{10}^{3.41}$	(Kirkevåg et al., 2013)

[a] Here W denotes the whitecap fraction.

Table 3. Comparison of global averages (median) of sea spray aerosol column burdens (C_{SSA}), all-sky sea spray aerosol optical depth, mass specific extinctions (ME), and sea spray atmospheric residence times between the three NorESM model runs.

Model run	C_{SSA} (mg m^{-2})	SSA optical depth (–)	SSA ME (m^2 g^{-1})	SSA residence time (h)
Current parameterisation (climatogy SST's)	7.44	0.0379	5.10	29.6
Current parameterisation (SST's fixed at 15 °C)	7.42	0.0383	5.16	29.2
Previous parameterisation	9.74	0.0302	3.10	10.0

Full Screen / Esc

Printer-friendly Version

Interactive Discussion

Figure 1. Mean particle **(a)** number size distribution, **(b)** surface size distribution, and **(c)** volume size distribution measured at different water temperatures. The solid lines represent the DMPS measurements ($D_p < 0.7\,\mu m$ electrical mobility diameter), while the dashed lines show the OPSS data ($D_p > 0.35\,\mu m$ optical equivalent diameter when $m = 1.54 - 0i$).
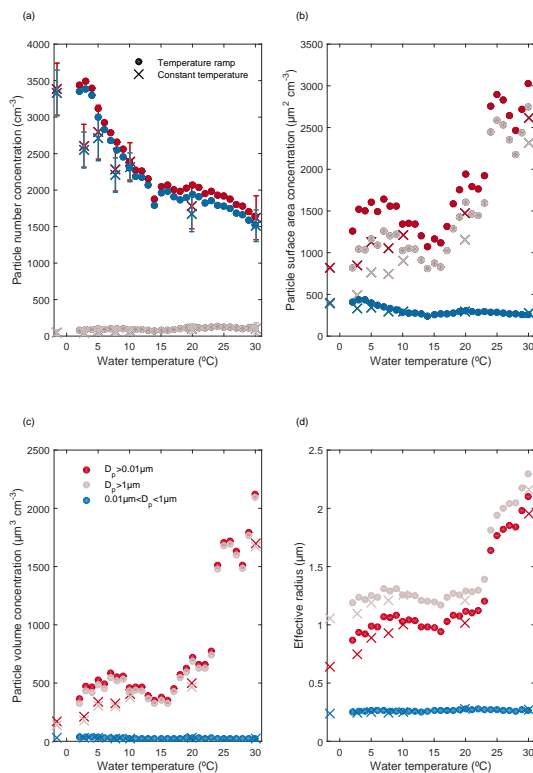
Figure 2. Integrated **(a)** number, **(b)** surface, and **(c)** volume as a function of water temperature for the constant water temperature experiments (crosses) and during the temperature ramp experiment (circles). One standard deviation (1σ) is shown for the integrated number concentration during the constant temperature experiments. Panel **(d)** plots the effective radius as a function of water temperature for all experiments.

Title Page

Abstract | Introduction

Conclusions | References

Tables | Figures

|◀ | ▶|

◀ | ▶

Back | Close

Full Screen / Esc

Printer-friendly Version

Interactive Discussion
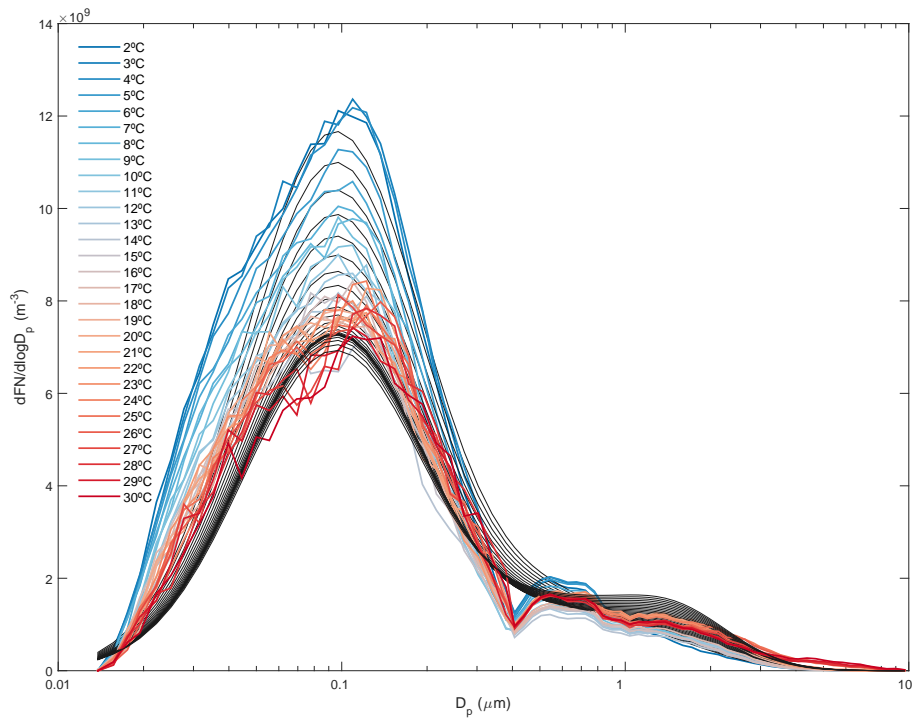
Figure 3. Mean aerosol number effective flux distribution of the corrected temperature ramp data (coloured lines) and corresponding lognormal fits constrained by fixed modal diameters and geometric standard deviations (black lines).

Title Page

Abstract | Introduction

Conclusions | References

Tables | Figures

|◄ | ►|

◄ | ►

Back | Close

Full Screen / Esc

Printer-friendly Version

Interactive Discussion
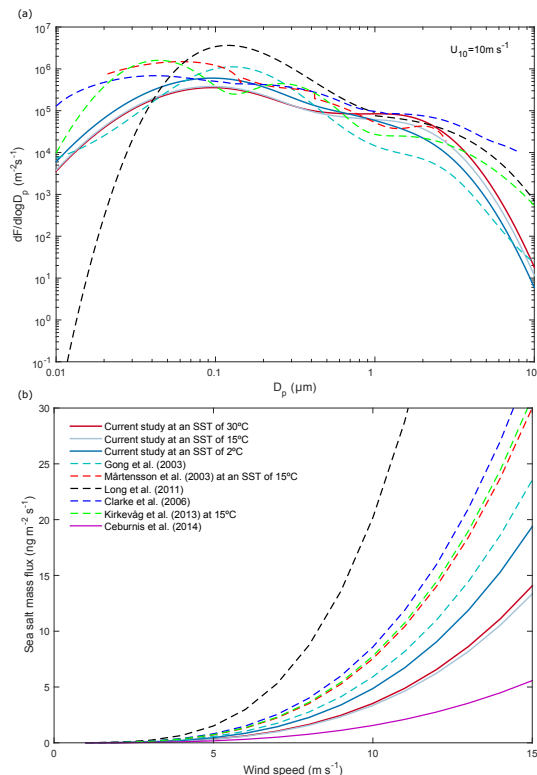
Figure 4. (a) The here derived sea spray source function (dF/d logD_p) for three different sea surface temperatures compared to the parameterisations of Mårtensson et al. (2003), Gong (2003), Long et al. (2011), and Clarke et al. (2006), as well as the source function previously implemented in the Earth system model, NorESM described by Kirkevåg et al. (2013) (see legend in panel **(b)**). Panel **(b)** plots integrated sub-micron (0.029 µm < D_p < 0.580 µm) sea salt mass fluxes as a function of wind speed measured at 10 m height for the same parameterisations shown in panel **(a)** as well as the fit to measured data reported by Ceburnis et al. (2014).

Full Screen / Esc

Printer-friendly Version

Interactive Discussion
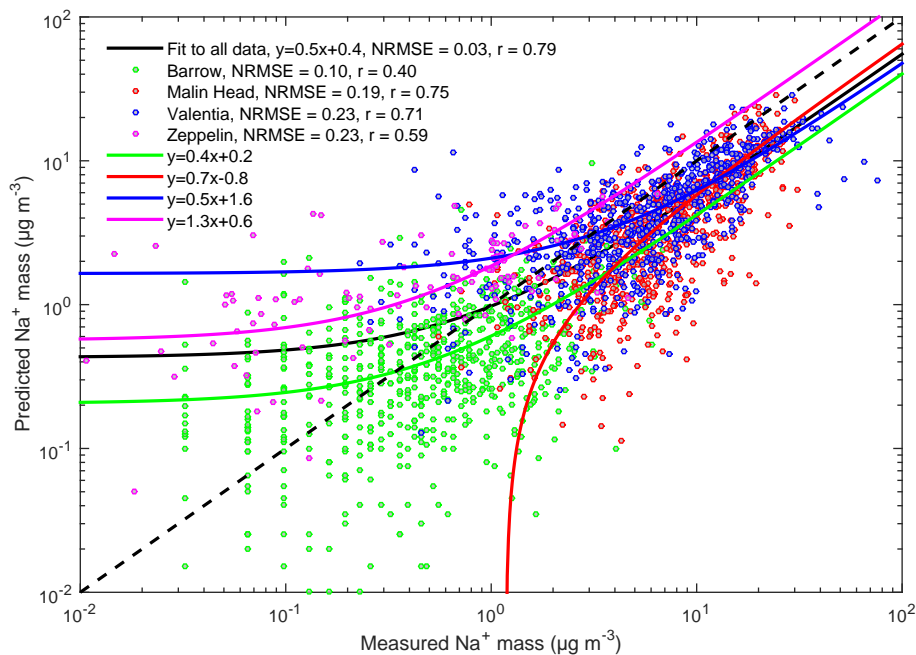
Figure 5. Comparison of FLEXPART modelled with measured Na^+ concentrations using the sea spray source function presented here for four stations included in the comparison by Grythe et al. (2014). Linear orthoganal fits are shown along with the Pearson's correlation coefficient for the whole dataset as well the individual stations. Also presented are the normalised root mean square errors (NRMSE) for the whole dataset as well as the individual stations. Here the NRMSE is the root mean square error normalised to the difference between the maximum and minimum measured values for the entire dataset or individual stations.
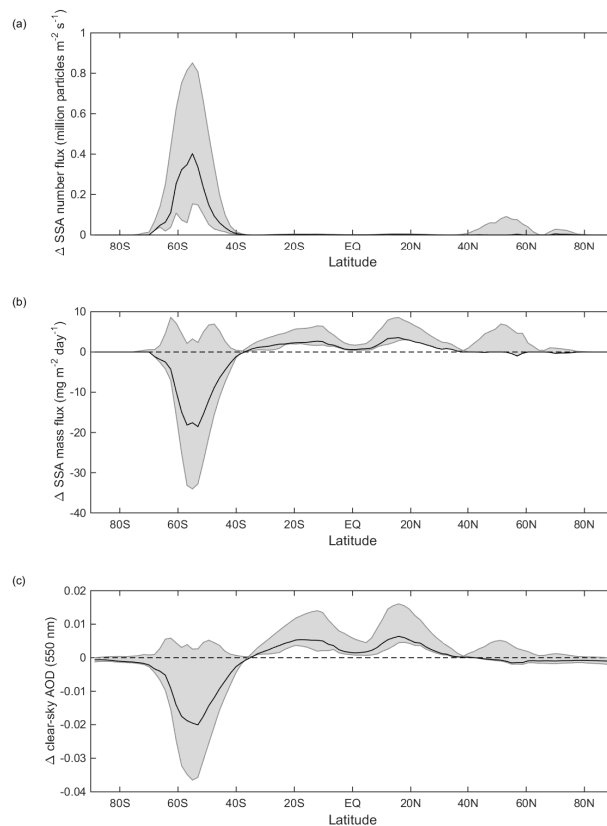
Figure 6. Zonal plots of the annually averaged (median) absolute difference in **(a)** SSA number fluxes, **(b)** SSA mass fluxes and **(c)** clear-sky aerosol optical depth at 550 nm between the parameterisation developed here with climatology sea surface temperatures and sea surface temperature fixed at 15 °C. Each plot was generated as the variable sea surface temperature simulation minus the fixed sea surface temperature simulation. Shaded areas represent 25th and 75th percentiles.

Title Page

Abstract | Introduction

Conclusions | References

Tables | Figures

|◄ | ►|

◄ | ►

Back | Close

Full Screen / Esc

Printer-friendly Version

Interactive Discussion
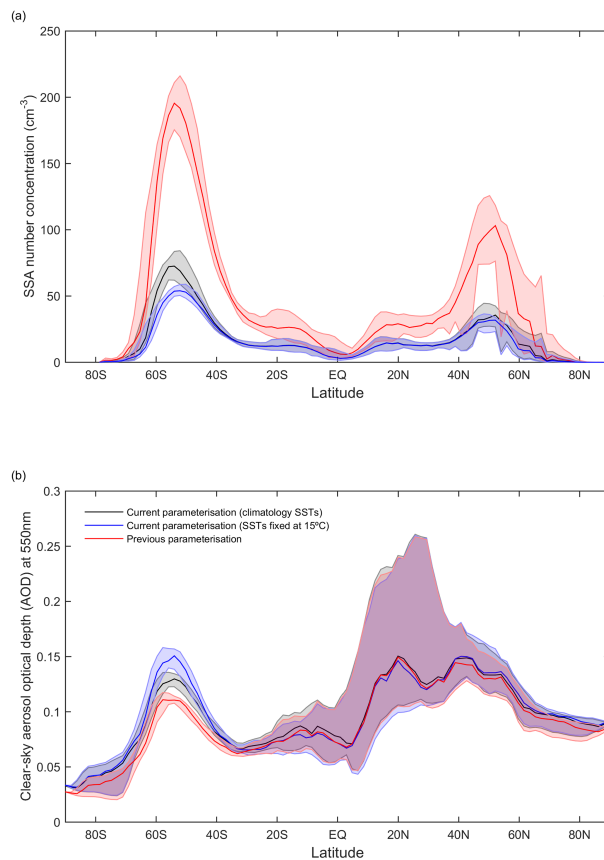
Figure 7. (a) Annually averaged (median) sea spray aerosol number concentration in the lowest model layer computed during the three NorESM runs. **(b)** Zonally and annually averaged clear-sky aerosol optical depth at 550 nm computed during the three NorESM runs (median). Shaded areas represent the 25th and 75th percentiles.

Title Page

Abstract | Introduction

Conclusions | References

Tables | Figures

|◄ | ►|

◄ | ►

Back | Close

Full Screen / Esc

Printer-friendly Version

Interactive Discussion
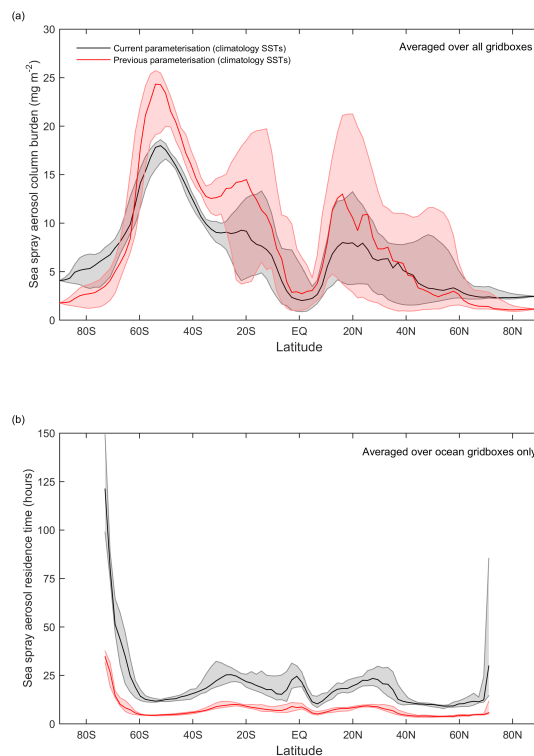
Figure 8. (a) Comparison of zonally (over all grid boxes) and annually averaged (median) sea spray aerosol column burden computed with the current parameterisation and the previous parameterisation (Kirkevåg et al., 2013). **(b)** Comparison of zonally (only ocean grid boxes) and annually averaged (median) sea spray aerosol residence time computed with the current parameterisation and the previous parameterisation (Kirkevåg et al., 2013). Shaded areas represent the 25th and 75th percentiles.